J. Fluid Mech. (1978), *vol.* 85, *part* 4, *pp.* 641–653
Printed in Great Britain

Experimental study of the velocity field in Rayleigh–Bénard convection

By M. DUBOIS AND P. BERGÉ

Commissariat à l'Energie Atomique, Division de la Physique, Centre d'Etudes Nucléaires de Saclay, B.P. 2, 91190 Gif-sur-Yvette, France

(Received 17 May 1976 and in revised form 31 August 1977)

Local velocity measurements performed in a convecting layer of fluid show that the velocity field can be described by a dominant fundamental velocity mode mixed with an increasing proportion of second and third harmonics as ϵ, the reduced distance to the convective threshold R_c, is increased from 0 to $\sim$ 10. The spatial and thermal dependences of the amplitudes of these different modes are reported and compared with theoretical predictions.

1. Introduction

When a horizontal layer of a pure expansible fluid is subjected to a vertical temperature difference ΔT greater than a critical value ΔT_c, this fluid becomes unstable if the lower part of the fluid is warmer than the upper part. That is, we are dealing with the so-called Rayleigh–Bénard instability.

Many investigators have studied the properties of this kind of instability, but unti recently only macroscopic measurements have been made (Koschmieder 1973). One might mention, for example, the studies of the structure and its evolution with ΔT by visualization of the convective rolls (Chen & Whitehead 1968; Krishnamurti 1968), and fine measurements of the variation of the Nusselt number when an increased gradient is applied to the fluid layer. But all these measurements, accurate as they are, give only a global view of the behaviour of the convecting fluid. An example is given by the fact that the measured Nusselt number has a transition only at ΔT_c and then increases monotonically with ΔT up to values greater than $200\Delta T_c$ (Koschmieder & Pallas 1974) though we know, from other observations, that convecting layers undergo several definite transitions: e.g. to three-dimensional motion, to time-dependent motion and eventually to turbulence (Busse & Whitehead 1971, 1974; Krishnamurti 1970; Bergé & Dubois 1974; Gollub *et al.* 1976; Ahlers 1974).

In order to find out more details about the convective properties, it is necessary to measure a local variable, such as the velocity or the temperature perturbation. Beautiful measurements of the latter (Farhadieh & Tankin 1974) have already been made. We report here our measurements of the velocity field and its dependence on the supercritical temperature gradient in the domain $R_c < R < 11R_c$. Here R is the Rayleigh number and R_c its critical value at the onset of thermoconvection:

$$R = \alpha g d^3 \Delta T / \nu K, \tag{1}$$

where α is the volume expansion coefficient, g is the gravitational acceleration, d is the depth of the fluid layer and ν and K are respectively the kinematic viscosity and thermal diffusivity of the fluid ($K = \lambda/\rho C_p$). We shall see that the velocity field can be

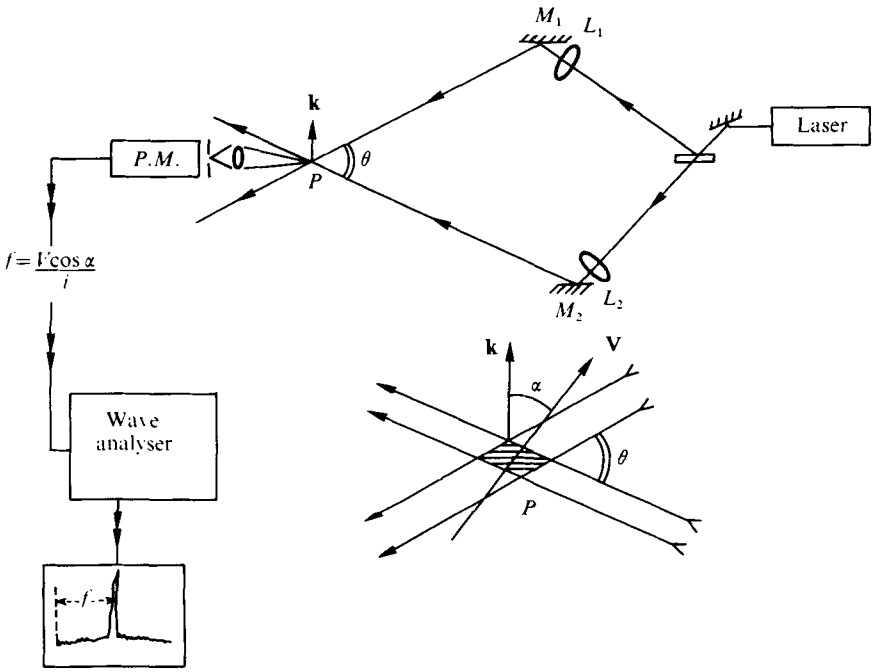

FIGURE 1. Experimental set-up. L_1, L_2 and M_1, M_2 are respectively lenses and mirrors; *P.M.* is the photomultiplier. **k** is the exterior bisector of the two beams.

described by a superposition of different spatial modes whose wavelengths correspond to the first few harmonics given by the linear stability analysis and we shall compare our results with those obtained from finite amplitude calculations.

2. The experimental set-up

The cell

The fluid is confined in a 10×3 cm rectangular Plexiglas frame whose depth is $d = 1$ cm. The horizontal boundaries below and above the frame are made of massive, 1 cm thick, copper plates; they are good heat conductors with

$$K_{Cu} \gg K_{fluid} \quad (K_{Cu} = 1{\cdot}12\,\mathrm{cm^2\,s^{-1}}).\dagger$$

Their temperatures are carefully regulated to within 10^{-2} °C by circulating water provided by two thermostatic baths. The temperature difference between the two plates is measured with an accurately calibrated differential thermocouple.

Velocity measurements

The local velocity in the fluid is measured by laser anemometry, the principle of which is well known (Wang 1972). A schematic diagram of our experimental set-up is shown in figure 1. Two parallel and coherent beams from the same laser (He–Ne, 5 mW) intersect and form interference fringes at their crossing point P. The fringe spacing is given by

$$i = \lambda'/2 \sin \tfrac{1}{2}\theta, \tag{2}$$

† We know from experiments (Bergé & Dubois 1974) and from calculations (Normand Pomeau & Vélarde 1977) that the results depend on the ratio K_{plate}/K_{fluid}.

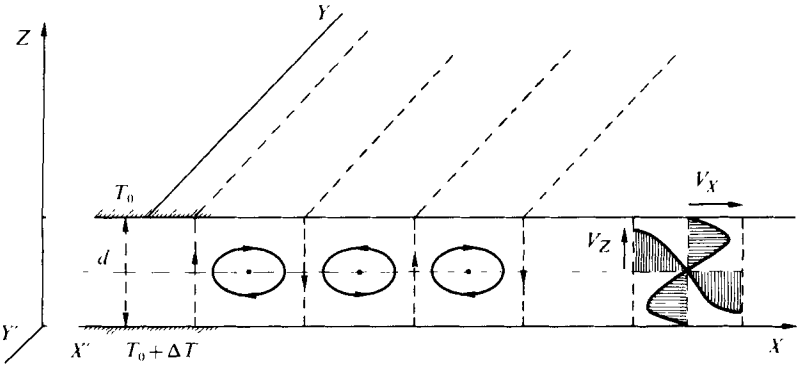

FIGURE 2. Schematic representation of two-dimensional rolls corresponding to the velocity field in the linear domain.

where λ' is the wavelength of the light and θ the angle between the two beams in the fluid. We choose $\theta \simeq 21°$ (in air) so that the two beams, which are in a vertical or in a horizontal plane, can enter the cell through the Plexiglas frame. In this case $i \simeq 1{\cdot}75\,\mu$m. The velocity measurements are made in a rather small volume of $0{\cdot}45 \times 0{\cdot}45 \times 3{\cdot}5$ mm^3, the beam diameter being reduced by lenses (L_1 and L_2 in figure 1). If particles cross the fringes, the scattered light is time modulated at the frequency $f = V_k/i$, where V_k is the projection of the particle velocity on the scattering vector **k** as shown in figure 1.

The laser beams are arranged such that **k** is parallel to the axis $X'X$ (V_X measurements) or the axis $Z'Z$ of the cell (V_Z measurements); $Z'Z$ is the vertical axis and $X'X$ the horizontal axis parallel to the long side of the frame (see figure 2).

Part of the light scattered at the point P is focused on a pin-hole in front of a photomultiplier and a real-time Fourier analyser gives directly the frequency f corresponding to the modulation of the photocurrent, from which we deduce V_k.

Physical properties of the fluid

In the experiments reported here, we used silicone oil, the physical properties of which are given in table 1. The Prandtl number $\sigma = \nu/K$ is about 930 at 25 °C. The viscosity ν and the refractive index n have been measured in our laboratory. The other parameters are taken from a table provided by the oil's manufacturer.

The flow pattern

It is well known (Schlüter, Lortz & Busse 1965; Davis 1968; Stork & Müller 1972) that in a rectangular box the convective structure just above onset consists of straight rolls parallel to the shorter side of the rectangular frame. In our geometry, whose aspect ratio is $\frac{1}{10}$ along $X'X$ and $\frac{1}{3}$ along $Y'Y$, we clearly observed this feature (Bergé 1975). For low supercritical Rayleigh numbers the rolls were set up preferentially with a wavelength $\Lambda \equiv \Lambda_c \sim 2d$. Λ remains constant in our cell up to $\epsilon \simeq 10\,[\epsilon = (R - R_c)/R_c]$. The experimental value of R_c determined from our velocity measurements is 1600 ± 100; the error is mainly due to the uncertainty in the physical constants of the oil.

Note, however, that structures with $\Lambda \neq \Lambda_c$ can be obtained and maintained in the same temperature range but that all the results reported here refer to structures with wavelength $\Lambda \equiv \Lambda_c$. Another important point is the fact that the structure is essentially two-dimensional:

T (°C)	ρ (g cm^{-3})	ν (cm^{2}s^{-1})	α (°C^{-1})	λ (cal cm^{-1} °C^{-1} s^{-1})	C_p (cal g^{-1})	K (cm^2 s^{-1})	n
25	0·960	1·056	$0{\cdot}96 \times 10^{-3}$	$(3{\cdot}7 \pm 0{\cdot}1) \times 10^{-4}$	$0{\cdot}337 \pm 0{\cdot}002$	$(1{\cdot}14 \pm 0{\cdot}02) \times 10^{-3}$	1·402
35	0·952	0·875				$(1{\cdot}15 \pm 0{\cdot}02) \times 10^{-3}$	1·398

TABLE 1

(*a*) V_X and V_Z (the horizontal velocity component parallel to the long side of the frame and the vertical component) are independent of Y;

(*b*) $V_Y \equiv 0$ (V_Y is the horizontal velocity component parallel to the short side of the frame).

We accurately checked point (*a*) for values of ϵ lower than 5. For $\epsilon > 5$, V_Z is slightly dependent on Y, this 'modulation' reaching 7 % at $\epsilon \sim 9{\cdot}5$. We performed all our measurements at $Y = \frac{1}{2}l$, i.e. at the middle of the horizontal cell width. The main problem of the three-dimensionality ($V_Y \neq 0$) will be discussed in a separate paper but we can mention here that in the same geometry a well-defined threshold exists for V_Y but is above the studied range of ϵ.

3. Experimental results

Our aim is to study the velocity field in the layer from measurements of the two velocity components V_X and V_Z. But the spatial arrangement of the two laser beams with respect to the cell allows us to measure the whole field only for the V_X component, since V_Z can be measured only in the vicinity of the midheight of the fluid layer ($Z \sim 0{\cdot}5d$). As we have reported earlier (Dubois 1976), the velocity field is perfectly reproducible from one roll to another (if we neglect those near the boundaries). Thus measurement of the velocity field along only one wavelength suffices to establish reliable data on the flow field.

The X dependence: Fourier analysis

Most of our measurements give the dependences $V_X = f(X)$ and $V_Z = f(X)$ at fixed values of Z, Y and ϵ, typical examples of which are shown in figures 3(*a*) and (*b*). A Fourier analysis is then performed on the experimental spatial dependences. We decompose the data into a sum of different spatial modes including the fundamental (here $\Lambda \equiv \Lambda_c$) and its first few harmonics ($\frac{1}{2}\Lambda_c, \frac{1}{3}\Lambda_c, \ldots$).

In the domain $0 < \epsilon < 10$, the three first spatial modes Λ_c, $\frac{1}{2}\Lambda_c$ and $\frac{1}{3}\Lambda_c$ are needed to fit the experimental points. We have, however, searched for the fourth and fifth harmonics, but could not establish their presence. Typical examples of our results are shown in figures 3(*a*) and (*b*). The quality of the fit between experimental data and the results of the Fourier analysis can be seen on these figures, where the solid line represents our calculated profile obtained from the relation

$$V_X(Z) = V_X^1(Z)\sin\frac{2\pi X}{\Lambda_c} + V_X^2(Z)\sin\left(\frac{4\pi X}{\Lambda_c} + \phi_2\right) + V_X^3(Z)\sin\left(\frac{6\pi X}{\Lambda_c} + \phi_3\right), \qquad (3)$$

in which the origin of the X axis is taken at one of the lateral boundaries of the fluid. The experimental data give $\phi_3 \equiv 0$ and $\phi_2 = \pm\pi$.

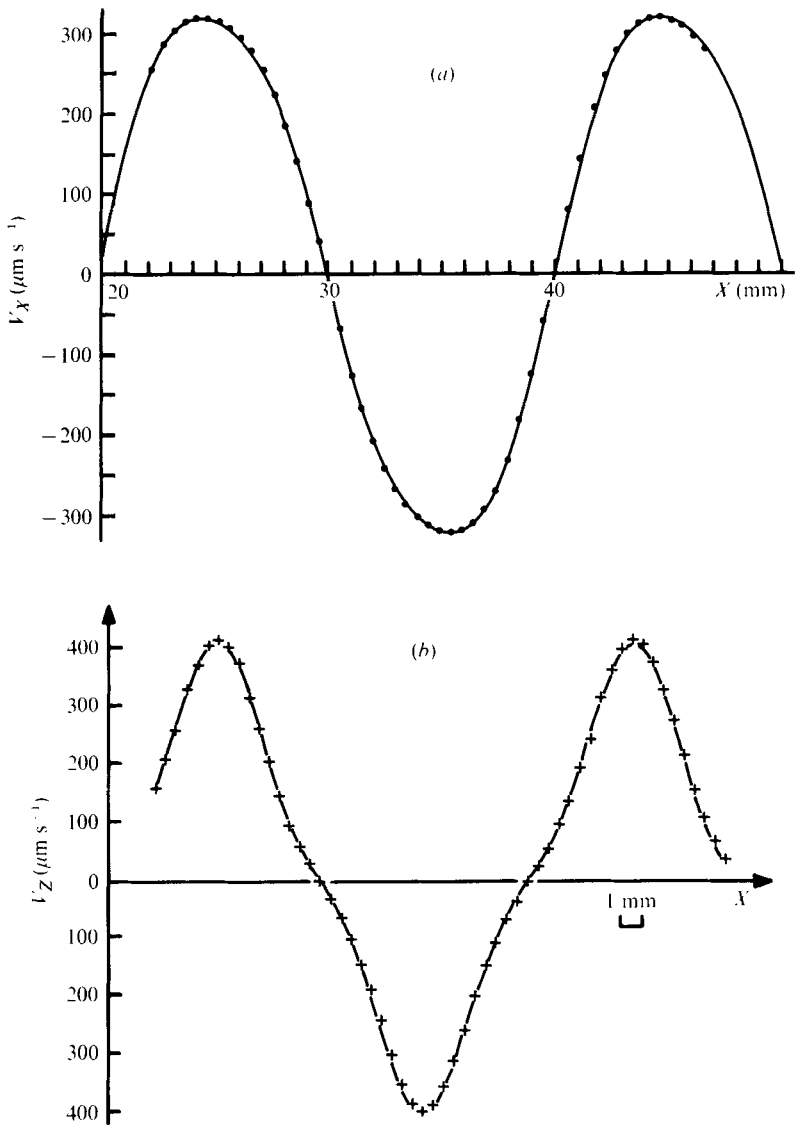

FIGURE 3. (*a*) Dependence of the horizontal component V_X of the velocity on X measured at $Z = Z^* = 0{\cdot}22d$; $\epsilon = 5{\cdot}76$. ●, experimental measurements; ——, computer best fit, with the following values: $V_X^1 = 337 \pm 10\,\mu\text{m}\,s^{-1}$, $V_X^2 = 13{\cdot}7 \pm 1\,\mu\text{m}\,\text{s}^{-1}$, $V_X^3 = 19 \pm 1\,\mu\text{m}\,\text{s}^{-1}$. (*b*) Dependence of the V_Z component on X compared with the computer best fit, which gives $V_Z^1 = 340 \pm 10\,\mu\text{m}\,\text{s}^{-1}$, $V_Z^2 = 1{\cdot}7 \pm 2\,\mu\text{m}\,\text{s}^{-1}$ and $V_Z^3 = 58 \pm 5\,\mu\text{m}\,\text{s}^{-1}$ ($Z = \frac{1}{2}d$, $\epsilon = 5{\cdot}67$).

$V_X^1(Z)$, $V_X^2(Z)$ and $V_X^3(Z)$ are the Fourier amplitudes of the different modes at the level Z. In the case of the curve shown on figure 3(*a*), measured at $Z = Z^* = 0{\cdot}22d$ (where V_X^1 is a maximum with respect to Z), $Y = \frac{1}{2}l$ and $\epsilon = 5{\cdot}76$, we obtained

$$V_X^1(Z^*) = 337 \pm 10\,\mu\text{m}\,\text{s}^{-1}, \quad V_X^2(Z^*) = 13{\cdot}7 \pm 1\,\mu\text{m}\,\text{s}^{-1}, \quad V_X^3(Z^*) = 19 \pm 1\,\mu\text{m}\,\text{s}^{-1}.$$

In the same way Fourier analysis of the curve shown on figure 3(*b*) ($Z = Z^{**} = 0{\cdot}5d$,

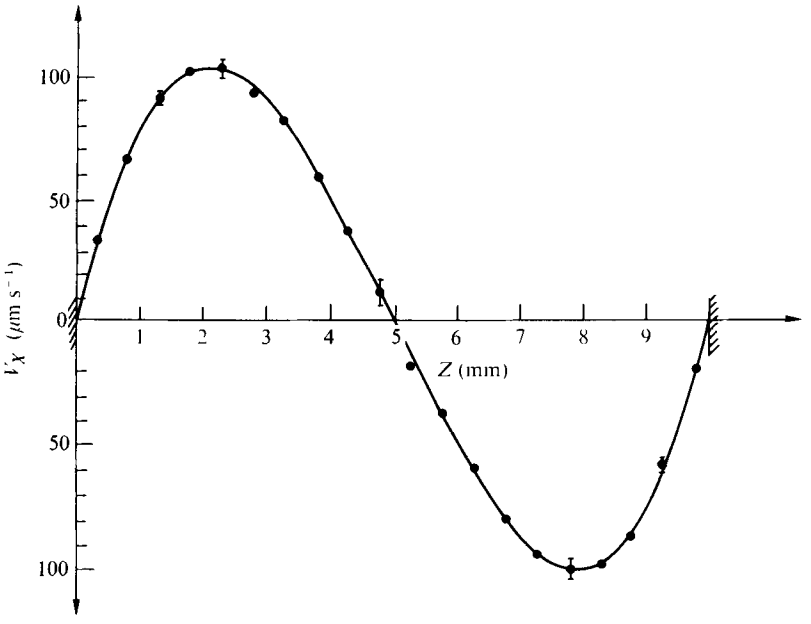

FIGURE 4. Dependence of the horizontal component $V_X = V_X^1$ on Z measured at $\epsilon = 0{\cdot}69$. $X = \frac{1}{4}(2k+1)\,\Lambda$ (k is an integer).

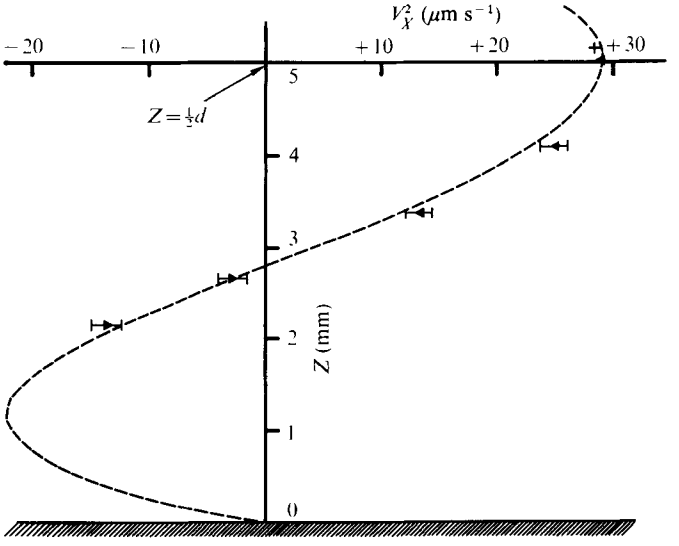

FIGURE 5. Measured amplitude of V_X^2 component plotted against Z at $\epsilon = 5{\cdot}75$. The dashed line represents the theoretical profile.

$Y = \frac{1}{2}l$, $\epsilon = 5{\cdot}67$) gives

$$V_Z^1(Z^{**}) = 340 \pm 10\,\mu\text{m s}^{-1}, \quad V_Z^2(Z^{**}) = 1{\cdot}7 \pm 2\,\mu\text{m s}^{-1}, \quad V_Z^3(Z^{**}) = 58 \pm 4\,\mu\text{m s}^{-1},$$

where V_Z obeys the general relation

$$V_Z(Z) = V_Z^1(Z)\cos\frac{2\pi X}{\Lambda_c} + V_Z^2(Z)\cos\frac{4\pi X}{\Lambda_c} + V_Z^3(Z)\cos\frac{6\pi X}{\Lambda_c}. \tag{4}$$

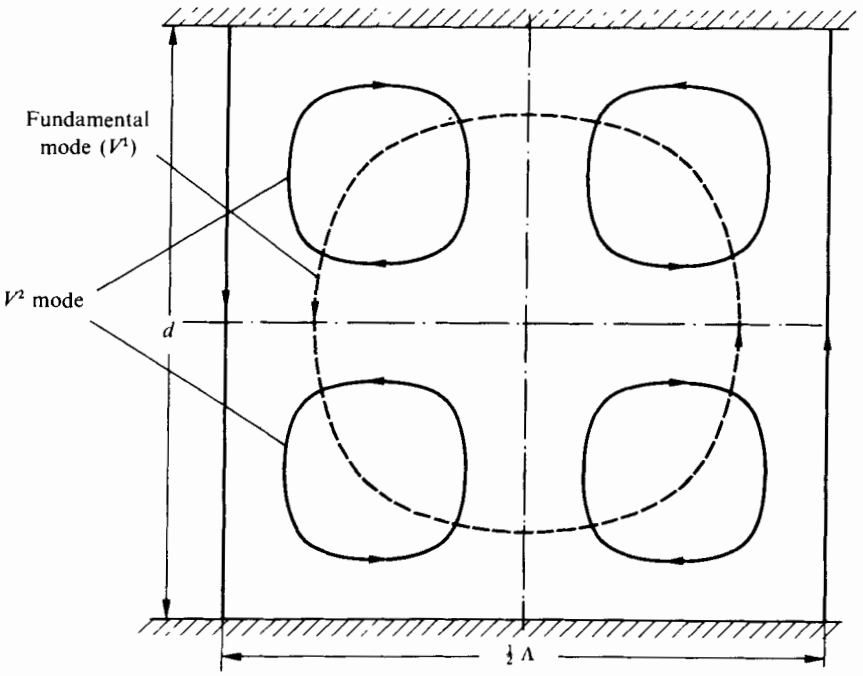

FIGURE 6. Schematic representation of the behaviour of the V^2 mode in comparison with the fundamental.

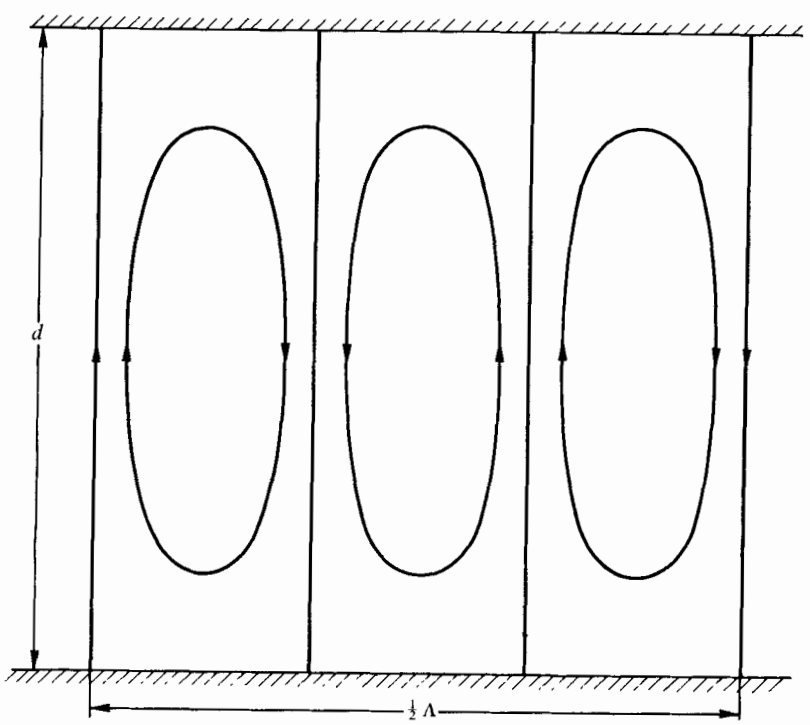

FIGURE 7. Schematic representation of the V^3 mode.

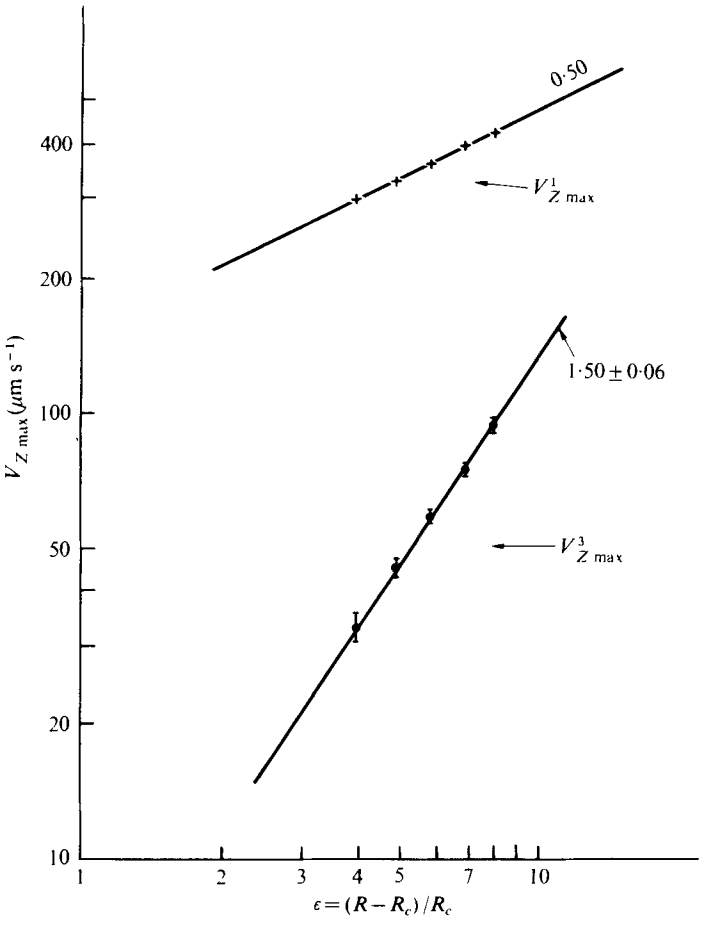

FIGURE 8. ϵ dependence of the maximum Fourier amplitudes $V^1_{Z\,max}$ and $V^3_{Z\,max}$.

The Z dependence of the velocity amplitudes

Fourier analysis of the dependences $V_X = f(X)$ and $V_Z = f(X)$ shows clearly the variation of the different harmonic amplitudes with X. But to find the full spatial variation of these amplitudes, it is necessary to examine the dependence of the velocity on Z.

At a given value of ϵ, we measured $V_X = f(X)$ at many different Z levels. Fourier analysis of each of these curves yields the variation $V^\alpha = f(Z)$, where V^α is the Fourier amplitude of mode α and $\alpha = 1$, 2 or 3. The results are shown in figures 4 and 5. For the first harmonic (figure 4), the dependence $V^1_X = f(Z)$ was obtained by direct measurement of V_X at a fixed value of X ($X = \frac{1}{4}(2k+1)\Lambda_c$, where V^1_X is a maximum with respect to X) for a low value of ϵ where the contributions of V^2 and V^3 are negligible (see below). One can see that $V_X(Z) \equiv V^1_X(Z)$ is a maximum at $Z = 0{\cdot}22d$ and zero at $Z = 0{\cdot}5d$.

Typical behaviour of $V^2_X(Z)$ is shown in figure 5; it appears that V^2_X goes through a maximum at the midheight ($Z = 0{\cdot}5d$) and has two zeros respectively at $Z = 0{\cdot}28d$ and $Z = 0{\cdot}72d$. If we disregard the boundary effects ($V_X = 0$ at $Z = 0, d$) the behaviour

of the second-harmonic component V_X^2 looks very much like that of the first, but displaced by one-half of the fluid depth. The dependence of V_X^3 on Z is quite similar to that of V_X^1, i.e. it vanishes at $Z = 0{\cdot}5d$ and goes through a maximum at $Z \simeq 0{\cdot}2d$.

By taking into account all the results concerning the spatial variation of the velocity, we can arrive at a simple description of the convective motion. The behaviour of the first harmonic can be accounted for by 'rolls' inscribed in squares of side d, the vorticity of the rolls being opposite in adjacent rolls. The second harmonic can be represented by four identical rolls superimposed on a fundamental roll as shown in figure 6, and the third harmonic by three rolls elongated along the Z axis (figure 7).

Variation of the V^α with ϵ

As explained above, the spatial dependence of the velocity field can be thought of as composed of a superposition of harmonic modes of different amplitude. So the characteristics of the total flow will depend on the relative amplitudes of these harmonic components. For a given value of ϵ, we know from our spatial analysis the maximum amplitude of each component V_X^α and V_Z^α; let us call this $V_{X\max}^\alpha$ or $V_{Z\max}^\alpha$ respectively, each corresponding to a specific point in the layer. Let us now see how these maximum values depend on ϵ.

In the midplane of the cell, we have

$$V_Z = V_Z^1(Z^{**})\cos\left(\frac{2\pi X}{\Lambda_c}\right) + V_Z^3(Z^{**})\cos\left(\frac{6\pi X}{\Lambda_c}\right), \tag{5}$$

V_Z^2 being zero for symmetry reasons and in agreement with our experimental results. Thus

$$V_Z^1(Z^{**}) = V_{Z\max}^1, \quad V_Z^3(Z^{**}) = V_{Z\max}^3. \tag{6}$$

These parameters were measured at different values of ϵ; they vary, as shown in figure 8, according to the power laws

$$V_{Z\max}^1 = (145 \pm 5)\,\epsilon^{0{\cdot}50\pm0{\cdot}02}\,\mu\mathrm{m\,s^{-1}}, \tag{7}$$

$$V_{Z\max}^3 = (4 \pm 0{\cdot}4)\,\epsilon^{1{\cdot}50\pm0{\cdot}06}\,\mu\mathrm{m\,s^{-1}}. \tag{8}$$

Similarly, the Fourier amplitudes $V_{X\max}^1$ and $V_{X\max}^3$ (measured at $Z = 0{\cdot}22d$) yield the same power laws:

$$V_{X\max}^1 = (132 \pm 4)\,\epsilon^{0{\cdot}50\pm0{\cdot}01}\,\mu\mathrm{m\,s^{-1}} \quad (\epsilon < 5), \tag{9}$$

$$V_{X\max}^3 = (1{\cdot}5 \pm 0{\cdot}3)\,\epsilon^{1{\cdot}50\pm0{\cdot}06}\,\mu\mathrm{m\,s^{-1}}. \tag{10}$$

Now, if we look at the behaviour of the second-harmonic terms, we remark that, in the midheight plane of the fluid layer ($Z^{**} = 0{\cdot}5d$), $V_X^1 = 0$ and $V_X^3 = 0$ (symmetry reasons) and V_X^2 is a maximum (see figure 5). So measurements of V_X at $Z^{**} = 0{\cdot}5d$ give directly V_X^2 (checked from periodicity with respect to X) and we find, as shown in figure 9, that

$$V_{X\max}^2 = (5{\cdot}3 \pm 0{\cdot}5)\,\epsilon^{0{\cdot}98\pm0{\cdot}04}\,\mu\mathrm{m\,s^{-1}}. \tag{11}$$

These results permit some pertinent remarks.

(*a*) In a relatively large domain, say $0 < \epsilon < 2$, the amplitudes of the second- and third-harmonic terms are very small compared with that of the fundamental. Thus in this domain the fundamental mode alone suffices to account for the convective motion: this domain may be called the 'linear domain'.

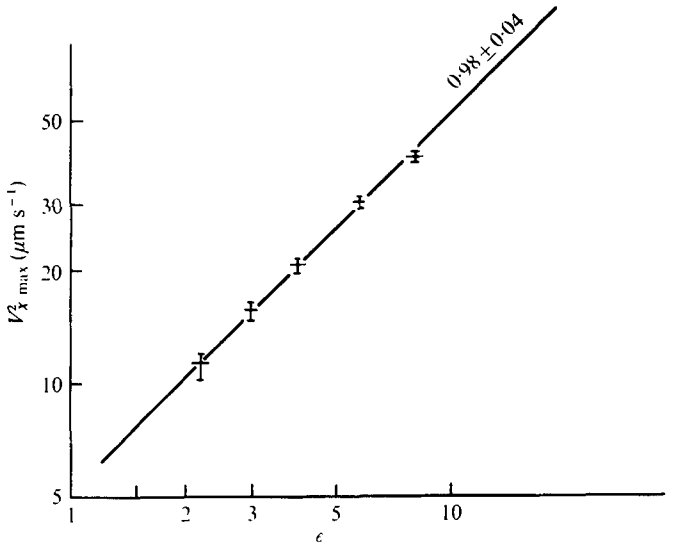

FIGURE 9. ϵ dependence of $V^2_{X\,\max}$ at $Z^{**} = \frac{1}{2}d$.

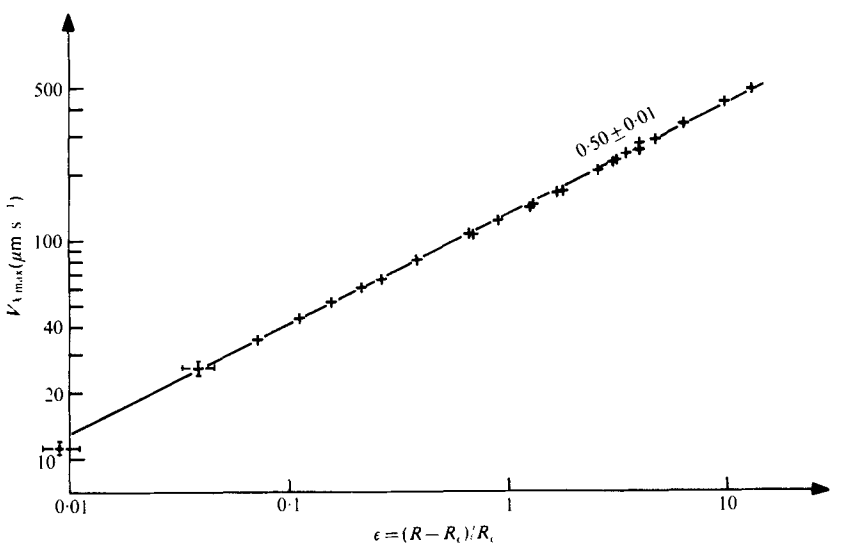

FIGURE 10. ϵ dependence of $V_{X\,\max}$.

(*b*) Comparison between the amplitudes of the horizontal and vertical components of the same harmonic is very instructive, because it expresses the conservation of the mass flow in a roll: $V^1_{X\max}$ is almost equal to $V^1_{Z\max}$ (square rolls, $\delta X = d$, $\delta Z = d$) and $V^3_{X\max}$ is about one-third of $V^3_{Z\max}$ (rectangular rolls, $\delta X = \frac{1}{3}d$, $\delta Z = d$) (see figure 7).

(*c*) $V^1_{X\max}$ does not exactly follow the power law (9) given above. For high values of ϵ we have to rewrite (9) as

$$V^1_{X\max} = 132\epsilon^{0\cdot5} + \Delta V^1_X \mu\mathrm{m\,s^{-1}} \tag{12}$$

with the approximate experimental relation

$$\Delta V^1_X \simeq 1\cdot5\epsilon^{1\cdot5}\,\mu\mathrm{m\,s^{-1}}. \tag{13}$$

The existence of this extra term explains a surprising result: in a large domain of ϵ, $V_{X\max}$, which contains first- and third-harmonic contributions, varies as $\epsilon^{0.5}$ (see figure 10), a behaviour which is expected for the first-harmonic mode alone. In fact, if we look at the respective phases of the different modes in figures 6 and 7, we can deduce that, at $X = \frac{1}{4}(2k+1)\Lambda$ and $Z = 0{\cdot}22d$, $V_X^2 = 0$ and

$$V_{X\max} = V^1_{X\max} - V^3_{X\max}. \tag{14}$$

$V^1_{X\max}$ is given by (12); thus we have

$$V_{X\,\max} = 132\epsilon^{0.5} + \Delta V^1_X - V^3_{X\max}.$$

From (10) and (13) we find that

$$\Delta V^1_X - V^3_{X\max} \simeq 0.$$

So $V_{X\max} = 132\epsilon^{0.5}$ as seen in figure 10.

The results obtained from Fourier analysis of figure 3(*a*) ($\epsilon = 5{\cdot}75$) give a good illustration of this behaviour:

$$V^1_{X\max} = 337\,\mu\mathrm{m\,s^{-1}},$$

from which we deduce $\Delta V^1_X = 17 \pm 2\,\mu\mathrm{m\,s^{-1}}$, which is approximately equal to $V^3_{X\max}$ ($= 19 \pm 1\,\mu\mathrm{m\,s^{-1}}$). Since this extra term ΔV^1_X is very small it is very difficult to study its variation with Z. Nevertheless, owing to its $\epsilon^{1.5}$ dependence, we are tempted to relate this term to another third-harmonic mode, with period Λ_c along X.

4. Comparison of our experimental results with finite amplitude calculations

Busse (1967) was the first to give the amplitudes of the local variables in a convective fluid. Recently, Norman *et al.* (1977) performed a complete calculation of the amplitudes and spatial dependences of the velocity field in the Rayleigh–Bénard problem. These calculations concern the first three harmonics and are valid for low supercritical Rayleigh numbers. They are based on the usual expansion in terms of a small parameter $\tilde{\epsilon}$ of the form

$$R = R_c + \tilde{\epsilon}R^{(1)} + \tilde{\epsilon}^2R^{(2)} + \tilde{\epsilon}^3R^{(3)} + \ldots, \tag{15}$$

where $R^{(1)} = R^{(3)} = 0$ in the case of two-dimensional rolls. In the same way,

$$V = \tilde{\epsilon}V_1 + \tilde{\epsilon}^2V_2 + \tilde{\epsilon}^3V_3 + \ldots, \tag{16}$$

where V is the amplitude of the velocity. These expansions, when restricted to the first terms in $\tilde{\epsilon}$ ($< \tilde{\epsilon}^4$), are valid only for low values of $\tilde{\epsilon}$, which is then equal to

$$(R_c/R^{(2)})^{\frac{1}{2}}\epsilon^{\frac{1}{2}} \quad [\epsilon = (R - R_c)/R_c].$$

Under this condition, the theoretical expression which gives the amplitude of $V^1_{Z\max}$ is

$$V^1_{Z\max} = 0{\cdot}96 \times 2^{\frac{1}{2}}a^2\frac{K}{d}\tilde{\epsilon} = 0{\cdot}96 \times 2^{\frac{1}{2}}a^2\frac{K}{d}\left[\frac{R_c}{R^{(2)}}\right]^{\frac{1}{2}}\epsilon^{\frac{1}{2}}, \tag{17}$$

where $a = (2\pi/\Lambda)d$ is the dimensionless wavenumber.

If $\Lambda = \Lambda_c$, we have $a = a_c = 3{\cdot}117$. We remark that, at a fixed value of ϵ, the velocity amplitude is dependent on only the physical parameter K (the thermal diffusivity of the convective fluid) and the depth d of the layer.

	First harmonic		Second harmonic		Third harmonic	
	$V^1_{Z\,\max}$	$V^1_{X\,\max}$	$V^2_{Z\,\max}$	$V^2_{X\,\max}$	$V^3_{Z\,\max}$	$V^3_{X\,\max}$
Theory (Normand *et al.*)	135	133	2·9	2·6	2·2	0·77
Theory (Busse)	138	133	—	5	3·8	—
Our experiments	145 ± 5	132 ± 4	—	$5{\cdot}3 \pm 0{\cdot}5$	$4 \pm 0{\cdot}4$	$1{\cdot}5 \pm 0{\cdot}3$

TABLE 2

Spatial dependence

Calculated spatial dependences $V^1_X = f(Z)$ and $V^2_X = f(Z)$ are shown in figure 4 (solid line) and figure 5 (dashed line) for the case of rigid–rigid boundaries with

$$V_Z = V_X = \theta = 0 \quad \text{at} \quad Z = 0, d$$

(θ is the temperature perturbation). We see that the agreement between the experimental and calculated dependences is very good; qualitative agreement is also found for the third-harmonic term.

Amplitudes of each velocity mode

All the results, experimental and calculated, are summarized in table 2, where values for $\epsilon = 1$ are given in $\mu\text{m s}^{-1}$. Following a remark of a referee, we include in this table the velocity amplitudes calculated from Busse's (1967) theory.

We can see that the agreement between the experimental and calculated results is very good for the first-harmonic terms. But the amplitudes $V^2_{\max}$ and $V^3_{\max}$ found experimentally are twice those calculated from perturbation theory (Normand *et al.*), while they are in agreement with values deduced from the Galerkin method (Busse).† On the other hand, we calculated the maximum amplitude of the fifth harmonic of the velocity from Busse's theory and found that even for $\epsilon \sim 10$ this amplitude is of the same order of magnitude as our experimental accuracy (2 or 3 %).

Dependence on ϵ

If we consider Landau mean-field theory, we expect that the amplitude of the fundamental velocity mode varies as $\epsilon^{0{\cdot}5}$. It follows that V^2 (given by second-order terms) varies as ϵ^1 and V^3 (given by third-order terms) as $\epsilon^{1{\cdot}5}$. These ϵ dependences can also be deduced by theoretical calculations from expansions like (16). If we look at the experimental results, we find it very interesting, but somethat surprising, to see that these power laws are followed even far from the threshold of the convective motion. In the entire domain studied V^1 remains proportional to $\epsilon^{0{\cdot}5}$, V^2 to ϵ^1 and V^3 to $\epsilon^{1{\cdot}5}$.

It is of interest to compare, at a high value of ϵ (say $\epsilon = 10$), the relative amplitudes of the three modes: $V^1_{Z\max} \simeq 460\,\mu\text{m s}^{-1}$, $V^2_{X\max} \simeq 48\,\mu\text{m s}^{-1}$ and $V^3_{Z\max} \simeq 132\,\mu\text{m s}^{-1}$. The contribution of the second harmonic remains comparatively low and, as seen above, does not affect the characteristic amplitudes of the velocity components $V_{X\max}$

† Note, however, that his values have ϵ dependences somewhat different to that observed and consequently the agreement with experimental amplitudes is not so consistent for higher values of ϵ, especially for the first-harmonic term.

and $V_{Z\max}$. On the other hand, the amplitude of the V^3 mode rapidly becomes important compared with that of the fundamental mode, in particular at the midheight of the fluid layer, where $V_{Z\max} = V^1_{Z\max} + V^3_{Z\max}$. In conclusion, the measurements reported here show that knowledge of a local variable such as the velocity is very important for the understanding of the convective properties. Moreover, comparison of the experimental amplitudes with calculated ones allowed us to perform a good test of different theories.

We thank C. Normand, Y. Pomeau and M. G. Velarde for their theoretical calculations, performed in parallel with our experimental work, and for stimulating discussions. We thank also L. de Sèze, who set up a Fourier-analysis computer program.

REFERENCES

AHLERS, G. 1974 *Phys. Rev. Lett.* **33**, 1185.

BERGÉ, P. 1975 *Fluctuations, Instabilities and Phase Transitions, Nato Adv. Study Inst.*, vol. B 11, p. 323. Plenum.

BERGÉ, P. & DUBOIS, M. 1974 *Phys. Rev. Lett.* **32**, 1041.

BUSSE, F. H. 1967 *J. Math. & Phys.* **46**, 140.

BUSSE, F. H. & WHITEHEAD, J. A. 1971 *J. Fluid Mech.* **47**, 305.

BUSSE, F. H. & WHITEHEAD, J. A. 1974 *J. Fluid Mech.* **66**, 67.

CHEN, M. M. & WHITEHEAD, J. A. 1968 *J. Fluid Mech.* **31**, 1.

DAVIS, S. H. 1968 *J. Fluid Mech.* **32**, 619.

DUBOIS, M. 1976 Thèse, Paris VI.

FARHADIEH, R. & TANKIN, R. S. 1974 *J. Fluid Mech.* **66**, 739.

GOLLUB, J. P., HULBERT, S. L., DOLNY, G. M. & SWINNEY, H. L. 1976 In *Photon Correlation Spectroscopy and Velocimetry* (ed. E. R. Pike & H. Z. Cummins). Plenum.

KOSCHMIEDER, E. L. 1973 *Adv. Chem. Phys.* **26**, 177.

KOSCHMIEDER, E. L. & PALLAS, S. G. 1974 *Inst. J. Heat Mass Transfer* **17**, 991.

KRISHNAMURTI, R. 1968 *J. Fluid Mech.* **33**, 445, 457.

KRISHNAMURTI, R. 1970 *J. Fluid Mech.* **42**, 295, 309.

MALKUS, W. V. R. & VERONIS, G. 1958 *J. Fluid Mech.* **4**, 225.

NORMAND, C., POMEAU, Y. & VELARDE, M. G. 1977 *Rev. Mod. Phys.* **49**, 581.

SCHLÜTER, A., LORTZ, D. & BUSSE, F. H. 1965 *J. Fluid Mech.* **23**, 129.

STORK, H. & MÜLLER, O. 1972 *J. Fluid Mech.* **54**, 599.

WANG, C. P. 1972 *J. Sci. Instrum.* **5**, 763.